**Ram Arti**
**Publishers**

# Static and Dynamic Load-Triggered Cascading Failure Mitigation for Storage Area Networks

## Guixiang Lyu
Department of Electrical and Computer Engineering,
University of Massachusetts, Dartmouth, MA, USA.
E-mail: glv@umassd.edu

## Liudong Xing
Department of Electrical and Computer Engineering,
University of Massachusetts, Dartmouth, MA, USA.
*Corresponding author*: lxing@umassd.edu

## Guilin Zhao
School of Computing & Artificial Intelligence,
Southwest Jiaotong University, Chengdu, Sichuan, China.
E-mail: guilinzhao@swjtu.edu.cn

**Abstract**
Storage area networks (SANs) are a widely used and dependable solution for data storage. Nevertheless, the occurrence of cascading failures caused by overloading has emerged as a significant risk to the reliability of SANs, impeding the delivery of the desired quality of service to users. This paper makes contributions by proposing both static and dynamic load-triggered redistribution strategies to alleviate the cascading failure risk during the mission time. Two types of node selection rules, respectively based on the load level and node reliability, are studied and compared. Based on the SAN component reliability evaluation using the accelerated failure-time model under the power law, the SAN reliability is evaluated using binary decision diagrams. A detailed case study of a mesh SAN is conducted to compare the performance of different cascading failure mitigation schemes using criteria of SAN reliability improvement ratio and resulting SAN reliability after the mitigation.

**Keywords-** Cascading failure, Dynamic scheme, Load redistribution, Mitigation, Static scheme.

## 1. Introduction
The rapid growth in the Internet of Things and telecommuting has induced big data and related storage issues (Jacob & Prakash, 2022; Hutanu et al., 2010). Storage area networks (SANs) have been adopted as one of the dependable storage solutions by enterprises like NetApp, Tintri, and IBM (Garber, 2012). SANs can provide any-to-any connections between servers and storage units within the network, leading to benefits of high throughput, low latency, and concurrent access (Sharma et al., 2022; Xing et al., 2017).

A major threat to the robust operation of SANs is cascading failures, which take place when a single incident causes a chain reaction, posing extensive damages to the system or even the environment (Li et al., 2022a; Liu et al., 2022; Mishra et al., 2020; Nguyen et al., 2021; Xing, 2021). Major causes of cascading failures include for example overload, device failures, human/operator mistakes, and cyber/physical attacks. Particularly, when overloading incurs the failure of one system component, the load of this failed component is reallocated to other available components, which may further incur overloading on these components in a domino manner, causing the entire system to crash or the outage of the service delivered by the system.

Intensive efforts have been expended in modeling and alleviating cascading failures in power systems; some studies were also found for high-performance computing systems. The cascading failure mechanisms have been studied using simulations, self-organized critical models, and complex network models (Bialek et al., 2016; Shi et al., 2010). The effects of cascading failures have been addressed in the system reliability analysis using methods such as topological methods, combinatorial methods, state space-based methods, and simulations (Xing, 2021). Different mitigation techniques based on source identification (Huang et al., 2016), vulnerable component detection (Ed-daoui et al., 2019), dependence of cascading failures on system operating (Liu et al., 2014) or topological (Dey et al, 2016) characteristics, interdependencies (Rahnamay-Naeini and Hayat, 2016), and optimal resource allocation (Ghorbani-Renani et al., 2020) have been put forward for power systems. Mitigation strategies based on redundant capacity (Dang et al., 2023), dynamic healing mechanisms (Al-Aqqad et al., 2023), resilience assessment (Li et al., 2022b), and selecting restoration strategies (Zhou et al., 2021) have also been proposed for different network systems. To the best of our knowledge, only little work has systematically researched the mitigation of cascading failures for SAN systems from the reliability perspective. Particularly, based on the investigation of loading on the SAN reliability in Lv and Xing (2021), load-redistribution based mitigation schemes were studied by Lv et al. (2023) where the redistribution was triggered by the overall SAN reliability dropping below a pre-defined level with the assumption that the loading of each SAN component is fixed before each redistribution (only considering the SAN reliability variation as mission time proceeds). This work aims to address the effects of changing loads and use load as a decision parameter in the design of the mitigation schemes.

Specifically, this work makes contributions by proposing load redistribution-based cascading failure mitigation schemes triggered by the overload of certain SAN switch (i.e., its workload reaches some threshold defined by the scheme). Both static and dynamic schemes are considered, which use the same fixed threshold and changing thresholds after each redistribution, respectively. The mitigation schemes should specify the nodes engaged in the load redistribution. Two types of node selection rules, respectively based on the load level and reliability of a node, are adopted. To demonstrate and compare the performance of different cascading failure mitigation schemes proposed in this work, we analyze the SAN component reliability using the accelerated failure-time model (AFTM) under the power law. We further analyze the SAN reliability using binary decision diagrams under different mitigation schemes. The comparisons are carried out using a detailed case study of a mesh SAN in terms of two objective criteria: SAN reliability improvement ratio and the resulting SAN reliability.

The rest of the paper is structured as follows: Section 2 briefs the AFTM. Section 3 covers the load redistribution mechanism under the proportional rule. Section 4 describes four mitigation schemes based on the static and dynamic thresholds as well as the two node selection rules. Section 5 presents the example mesh SAN system used in the case studies. Section 6 compares the different mitigation schemes using the case study. Section 7 investigates the effects of the step value on the performance of the proposed dynamic mitigation schemes. Section 8 gives conclusions and points out several future research problems.

## 2. The AFTM Model
We apply the AFTM to model the effects of workload on a device's reliability behavior (Kay and Kinnersley, 2002; Levitin and Amari, 2009). Specifically, under the AFTM, the reliability of a component is a function of mission time $t$ and loading $L$ as formulated in Equation (1).

$$R(t, L) = R_0(t\phi(L)) \tag{1}$$

In Equation (1), $R_0$ denotes the baseline reliability function. $\phi(L)$ denotes a multiplicative factor that is utilized for reflecting diverse stress levels under different workloads. For a single type of workload, $\phi(L)$ under the power law is defined in Equation (2) with $\alpha$ being the effect parameter.

$$\phi(L) = L^\alpha \tag{2}$$

If the baseline time-to-failure follows the exponential distribution, according to Equation (1) and Equation (2), the reliability function $R(t, L)$, unreliability function $F(t, L)$, and failure rate $\lambda(L)$ of a component subject to workload $L$ can be calculated as

$$R(t, L) = e^{-\lambda(t\phi(L))} = e^{-\lambda t L^\alpha}; F(t, L) = 1 - e^{-\lambda t L^\alpha}; \lambda(L) = \frac{F'(t,L)}{R(t,L)} = L^\alpha \lambda \tag{3}$$

## 3. Load Redistribution Mechanism

The load is redistributed based on the node degrees (Wang et al., 2008). There are two ways: proportional and inverse-proportional (Lv et al., 2023), where during the redistribution process, a SAN node with a greater node degree tends to receive more workload under the proportional rule, but less under the inverse-proportional rule. The proportional rule is adopted in this work and reviewed in this section.

Consider node $k$ whose workload is to be redistributed. Let $N_k$ denote a set containing node $k$ and all its neighboring nodes. Consider any node $j$ in the set $N_k$. Let $d_j$ denote the degree of node $j$. Then the weight of node $j \in N_k$ is given by Equation (4) (Harpel et al., 1997), where $\beta$ is a tunable parameter controlling the strength of the initial workload. Note that the weight of node $j \notin N_k$ is simply 0.

$$\Pi_j = \frac{d_j^\beta}{\sum_{m \in N_k} d_m^\beta} \tag{4}$$

The actual workload reallocated from node $k$ to node $j$ is given as

$$\Delta L_{jk} = L_k \Pi_j \tag{5}$$

Thereby, after the redistribution of node $k$'s workload, the updated workload of node $j$ (different from node $k$) is given by adding the extra workload from node $k$ to its original load $L_j$, that is,

$$\tilde{L}_j = L_j + \Delta L_{jk} \tag{6}$$

The updated workload of node $k$ is given by

$$\tilde{L}_k = \Delta L_{kk} \tag{7}$$

When workloads of multiple nodes in set $\Phi$ need to be redistributed simultaneously, by extending Equation (6) we calculate the updated workload of any node $j$ not belonging to $\Phi$ after reallocating workloads of all nodes in $\Phi$ as

$$\tilde{L}_j = L_j + \sum_{k \in \Phi} \Delta L_{jk} \tag{8}$$

and the updated load of any node $k$ in $\Phi$ as

$$\tilde{L}_k = \sum_{y \in \Phi} \Delta L_{ky} \tag{9}$$

## 4. Proposed Load Threshold-Triggered Mitigation Strategies

This section introduces load-triggered mitigation strategies, where in the event of a switch's load reaching a pre-defined threshold, we strategically reallocate the load from a set of nodes selected based on certain rule. Two different selection rules are considered: *load-sensitive* and *reliability-sensitive*, where nodes with the top $u$ highest load levels and nodes with the top $w$ lowest reliability values are

chosen for load reallocation, respectively. With the load reallocation from those top vulnerable nodes, the overloading and thus the risk of cascading failures can be effectively controlled.

In addition, we consider both static and dynamic load thresholds. Under the static type, a constant load threshold is used for triggering the load reallocation during the entire mission time. Under the dynamic type, the load threshold triggering the reallocation is dynamically adjusted after each load reallocation procedure is carried out. In particular, in the case studies of Section 6 and Section 7, the threshold is decreased by a constant step value $s$ to be used for triggering the next load reallocation during the mission.

**Table 1** summarizes the mitigation strategies based on the two node selection rules (load-sensitive and reliability-sensitive) and two types of thresholds (static and dynamic).

**Table 1.** Proposed load threshold-triggered mitigation strategies.

|  | Reliability-sensitive | Load-sensitive |
|---|---|---|
| **Static Threshold** | Scheme 1 | Scheme 2 |
| **Dynamic Threshold** | Scheme 3 | Scheme 4 |

## 5. Illustrative Example

**Figure 1** illustrates an example of a mesh SAN used for the comparative study of the proposed mitigation schemes in **Table 1**. There are two servers ($Sr_1$ and $Sr_2$) that are hosts providing data services as well as two storage arrays ($Sa_1$ and $Sa_2$). The SAN also contains five switches ($Sw_1$, $Sw_2$, $Sw_3$, $Sw_4$, $Sw_5$) that facilitate any-to-any communications between the servers and the storage arrays.
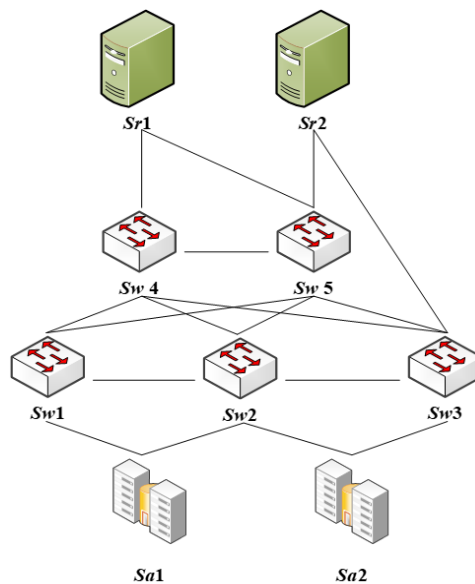


**Figure 1.** A mesh SAN.

It is assumed that only switches participate in the load allocations. Thereby, a switch's degree is defined as the number of links connecting this switch to other switches excluding links to servers and storage arrays. In the example SAN, the five switches have node degree of $d_{sw1}=3$, $d_{sw2}=4$, $d_{sw3}=3$, $d_{sw4}=4$, and $d_{sw5=}4$.

**Table 2** gives the baseline failure rate $\lambda$ and initial load $L_0$ applied for the five switches. Based on technical specifications of products in the industry (EMC Corporation, 2009; DELL EMC Corporation, 2019; Simache and Kaaniche, 2005), the failure rates of the servers ($Sr_1$, $Sr_2$) and storage arrays ($Sa_1$, $Sa_2$) are assumed to be 4.756469781e-11 per hour in this work (Lv and Xing, 2021).

**Table 2.** Baseline failure rate and initial load for the five switches.

| Switch | Failure rate $\lambda$ (per hour) | Initial load $L_0$ |
|--------|-----------------------------------|--------------------|
| $Sw_1$ | 3.0e-6 | 15 |
| $Sw_2$ | 5.0e-6 | 50 |
| $Sw_3$ | 3.0e-5 | 5 |
| $Sw_4$ | 3.0e-6 | 1 |
| $Sw_5$ | 3.5e-6 | 8 |

The SAN reliability is used as the key performance metric for comparing the proposed mitigation strategies, which is defined as the probability that at least one server can communicate with at least one storage array through an operational path formed by the switches. As the SAN reliability modeling and analysis are not contributions of this work, we only highlight the key model and concept to make the paper self-contained. Readers may refer to Lv et al. (2023) and Xing et al. (2014) for the detailed reliability analysis.

The example SAN can be modeled using the fault tree of **Figure 2**, where the SAN failure can be attributed to the server failure, the storage array failure and the path failure. The server failure takes place when both $Sr_1$ and $Sr_2$ are down; each server is down if the server itself fails or the switches providing the connection of the server to the rest of the SAN are down. Similarly, the storage array failure takes place when both $Sa_1$ and $Sa_2$ are down; each storage array is down if the array itself fails or the switches providing the connection of the array to the rest of the SAN are down. The path failure takes place if $Sw_1$, $Sw_2$, and $Sw_3$ all fail or $Sw_3$, $Sw_4$, and $Sw_5$ all fail. The fault tree in **Figure 2** can be converted to the binary decision diagram (Xing and Amari, 2015; Xing and Dugan, 2002), which is then evaluated to obtain the SAN unreliability as Equation (16) of Lv et al. (2023). This equation is used in later sections for the SAN reliability assessment.
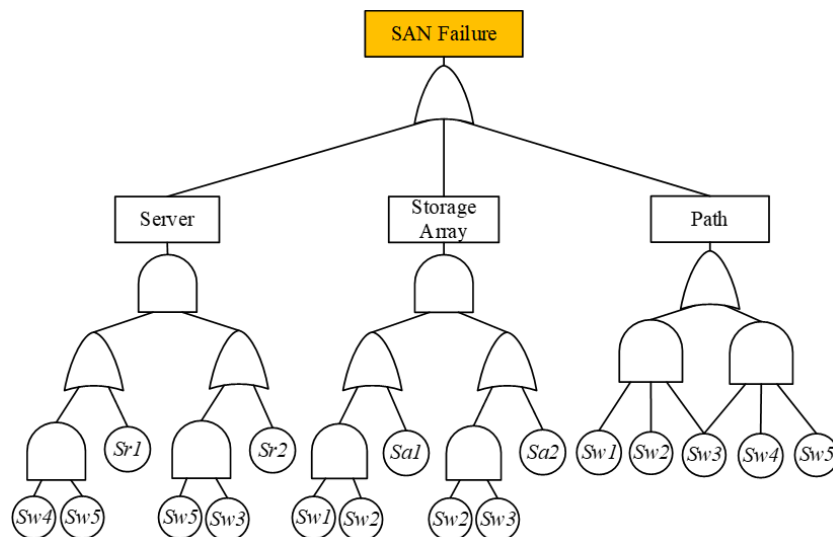


**Figure 2.** Fault tree of the example mesh SAN.

## 6. Performance Comparisons

This section evaluates and compares the performance of the proposed mitigation schemes in **Table 1**. During the studies, the load on $Sw_2$ serves as the triggering condition with the threshold of 50 in the static-threshold scheme (i.e., scheme 1 and scheme 2). In the dynamic-threshold schemes (i.e., scheme 3 and scheme 4), the value of $s$ is 5, that is, after each reallocation, the load threshold of $Sw_2$ for triggering the next load redistribution is decreased by 5.
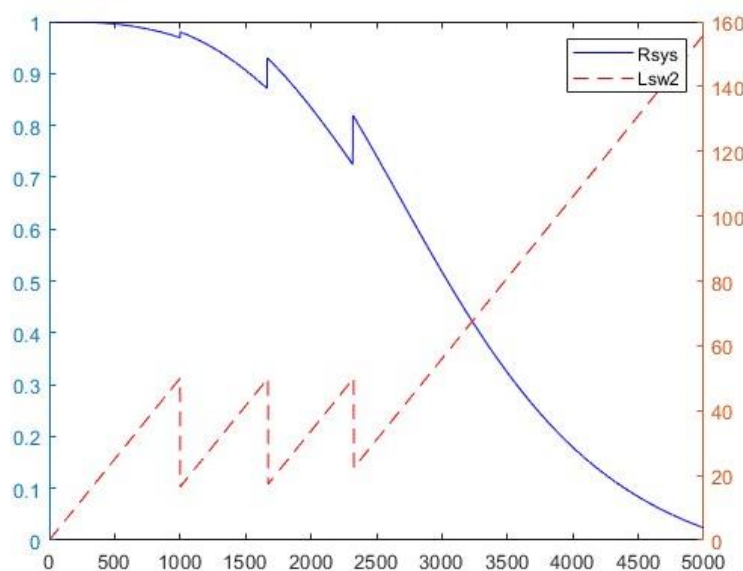
### 6.1 Scheme 1

To study the SAN reliability behavior under scheme 1, we increase the load of $Sw_2$ from 0 to 50 as mission time $t$ proceeds based on the function in Equation (10) while using the initial load values in **Table 2** for all other switches.

$$L_{Sw_2} = 0.05 \times t \tag{10}$$

At $t_1 = 1000h$, the load of $Sw_2$ reaches the threshold of 50, triggering the load redistribution. After the redistribution, $Sw_2$'s load drops to 16.44. Similarly, following the same function Equation (10) more load is added to $Sw_2$ until its load reaches 50 again at $t_2 = 1671h$, triggering the second load redistribution. After this redistribution, $Sw_2$'s load drops to 19.03. Then again according to Equation (10) more load is added to $Sw_2$ until its load reaches 50 again at $t_3 = 2290h$, triggering the third load redistribution. After this redistribution, $Sw_2$'s load drops to 23.02.

**Figure 3** illustrates the load changes of $Sw_2$ and the SAN reliability as the mission time proceeds. **Table 3** summarizes the load values of the five switches as well as the SAN reliability before and after each load redistribution under scheme 1, where the switches with the top three lowest reliabilities are selected for each load redistribution. During the first redistribution, $Sw_1$, $Sw_2$ and $Sw_3$ are selected; during the second redistribution, $Sw_2$, $Sw_3$ and $Sw_5$ are selected; during the third redistribution, $Sw_2$, $Sw_3$ and $Sw_4$ are selected (as highlighted in **Table 3**). The updated load values are evaluated using the formula of Section 3. The switch reliabilities are evaluated using Equation (3), and the entire SAN reliability is evaluated using Equation (16) of Lv et al. (2023).



**Figure 3.** The changes of SAN reliability and load of $Sw_2$ under scheme 1.
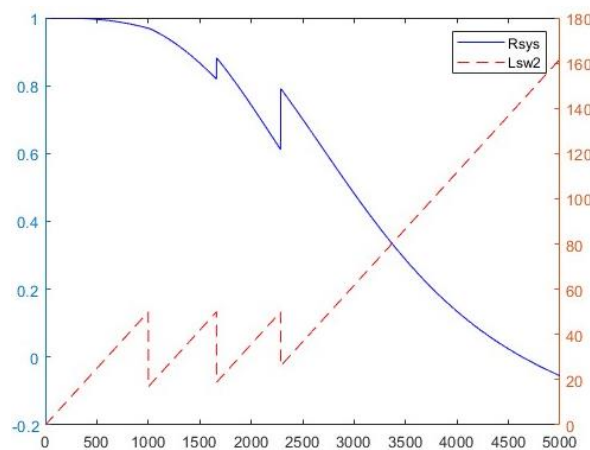
## 6.2 Scheme 2

Similarly, to study the SAN reliability behavior under scheme 2, we increase the load of $Sw_2$ from 0 to 50 as mission time $t$ proceeds based on Equation (10) while using the initial load values in **Table 2** for all other switches. At $t_1 = 1000h$, the load of $Sw_2$ reaches the threshold of 50, triggering the load redistribution. After the redistribution, $Sw_2$'s load drops to 16.89. Then, following Equation (10) more load is added to $Sw_2$ until its load reaches 50 again at $t_2 = 1663h$, triggering the second load redistribution. After this redistribution, $Sw_2$'s load drops to 18.84. Then again according to Equation (10) more load is added to $Sw_2$ until its load reaches 50 at $t_3 = 2286h$, triggering the third load redistribution. After this redistribution, $Sw_2$'s load drops to 25.93.

**Figure 4** illustrates the load changes of $Sw_2$ and the SAN reliability as the mission time proceeds. **Table 4** summarizes the load values of the five switches as well as the SAN reliability before and after each load redistribution under scheme 2, where the switches with the top three highest loads are selected for each load redistribution. During the first redistribution, $Sw_1$, $Sw_2$ and $Sw_5$ are selected; during the second redistribution, $Sw_2$, $Sw_4$ and $Sw_5$ are selected; during the third redistribution, $Sw_1$, $Sw_2$ and $Sw_3$ are selected (as highlighted in **Table 4**).

**Table 3.** Load and reliabilities of all the switches and the entire SAN under scheme 1.

| | Before redistribution | | | | | |
|---|---|---|---|---|---|---|
| | $t_1 = 1000h$ | | $t_2 = 1671h$ | | $t_3 = 2290h$ | |
| | Load | Reliability | Load | Reliability | Load | Reliability |
| $Sw_1$ | 15 | 0.9560405 | 11.33 | 0.9448019 | 23.74 | 0.8495677 |
| $Sw_2$ | 50 | 0.7791900 | 50 | 0.6589971 | 50 | 0.5646931 |
| $Sw_3$ | 5 | 0.8608370 | 9.33 | 0.6265041 | 14.27 | 0.3752358 |
| $Sw_4$ | 1 | 0.9970074 | 17.44 | 0.9163136 | 36.48 | 0.7784236 |
| $Sw_5$ | 8 | 0.9724155 | 24.44 | 0.9083570 | 19.03 | 0.8585798 |
| $R_{sys}$ | | 0.9692600 | | 0.8698263 | | 0.7069741 |
| | After redistribution | | | | | |
| | Load | Reliability | Load | Reliability | Load | Reliability |
| $Sw_1$ | 11.33 | 0.9666043 | 23.74 | 0.8878601 | 38.15 | 0.7695110 |
| $Sw_2$ | 16.44 | 0.9213730 | 19.03 | 0.8534225 | 23.02 | 0.7847972 |
| $Sw_3$ | 9.33 | 0.7559953 | 14.27 | 0.4891280 | 17.27 | 0.3055126 |
| $Sw_4$ | 17.44 | 0.9490621 | 36.48 | 0.8329785 | 23.02 | 0.8537628 |
| $Sw_5$ | 24.44 | 0.9180806 | 19.03 | 0.8947217 | 42.06 | 0.7139603 |
| $R_{sys}$ | | 0.9797991 | | 0.9162827 | | 0.8229352 |



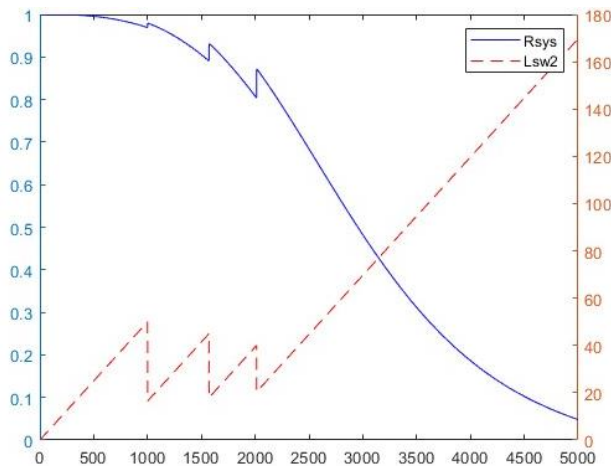**Figure 4.** The changes of SAN reliability and load of $Sw_2$ under scheme 2.

## 6.3 Scheme 3

To study the SAN reliability behavior under the dynamic scheme 3, we increase the load of $Sw_2$ from 0 to 50 as mission time $t$ proceeds based on Equation (10) while using the initial load values in **Table 2** for all other switches. At $t_1 = 1000$h, the load of $Sw_2$ reaches the initial threshold of 50, triggering the load redistribution. After the redistribution, $Sw_2$'s load drops to 16.44. Following Equation (10), more load is added to $Sw_2$ until its load reaches the new threshold (50-$s$) =45 at $t_2 = 1571$h, triggering the second load redistribution. After this redistribution, $Sw_2$'s load drops to 17.92. Then more load is added to $Sw_2$ until its load reaches the next new threshold (45-$s$) =40 at $t_3 = 2013$h, triggering the third load redistribution. After this redistribution, $Sw_2$'s load drops to 20.33.

**Figure 5** illustrates the load changes of $Sw_2$ and the SAN reliability as the mission time proceeds. **Table 5** summarizes the load values of the five switches as well as the SAN reliability before and after each load redistribution under scheme 3, where the switches with the top three lowest reliabilities are selected for each load redistribution. During the first redistribution, $Sw_1$, $Sw_2$ and $Sw_3$ are selected; during the second redistribution, $Sw_2$, $Sw_3$ and $Sw_5$ are selected; during the third redistribution, $Sw_2$, $Sw_3$ and $Sw_4$ are selected (as highlighted in **Table 5**).

**Table 4.** Load and reliabilities of all the switches and the entire SAN under scheme 2.

| | Before redistribution | | | | | |
|---|---|---|---|---|---|---|
| | $t_1 = 1000$h | | $t_2 = 1663$h | | $t_3 = 2286$h | |
| | Load | Reliability | Load | Reliability | Load | Reliability |
| $Sw_1$ | 15 | 0.9560405 | 12.67 | 0.9387970 | 26.80 | 0.8321949 |
| $Sw_2$ | 50 | 0.7791900 | 50 | 0.6600711 | 50 | 0.5652095 |
| $Sw_3$ | 5 | 0.8608370 | 14.67 | 0.4812925 | 28.80 | 0.1389021 |
| $Sw_4$ | 1 | 0.9970074 | 17.89 | 0.9146681 | 18.84 | 0.8788467 |
| $Sw_5$ | 8 | 0.9724155 | 16.88 | 0.9064289 | 18.84 | 0.8601324 |
| $R_{sys}$ | | 0.9692600 | | 0.8196209 | | 0.6120918 |
| | After redistribution | | | | | |
| | Load | Reliability | Load | Reliability | Load | Reliability |
| $Sw_1$ | 12.67 | 0.9627495 | 26.80 | 0.8729977 | 13.69 | 0.9104077 |
| $Sw_2$ | 16.89 | 0.9193299 | 18.84 | 0.8557942 | 25.93 | 0.7439769 |
| $Sw_3$ | 14.67 | 0.6443199 | 28.80 | 0.2379289 | 14.09 | 0.3805844 |
| $Sw_4$ | 17.89 | 0.9477988 | 18.84 | 0.9103430 | 44.77 | 0.7356986 |
| $Sw_5$ | 16.88 | 0.9426578 | 18.84 | 0.8962020 | 44.77 | 0.6990098 |
| $R_{sys}$ | | 0.9702458 | | 0.8828703 | | 0.7932698 |



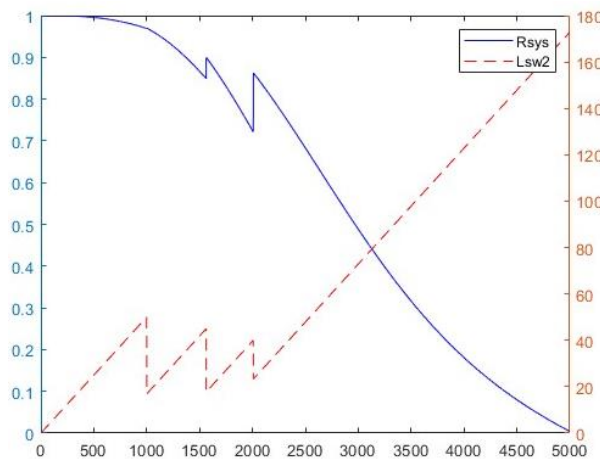**Figure 5.** The changes of SAN reliability and load of $Sw_2$ under scheme 3.

## 6.4 Scheme 4

Similarly, to study the reliability behavior under the dynamic scheme 4, we increase the load of $Sw_2$ from 0 to 50 as mission time $t$ proceeds based on Equation (10) while using initial load value in **Table 2** for all other switches. At $t_1 = 1000$h, the load of $Sw_2$ reaches the initial threshold of 50, triggering the load redistribution. After the redistribution, $Sw_2$'s load drops to 16.89. Following Equation (10), more load is added to $Sw_2$ until its load reaches the new threshold 45 at $t_2 = 1562$h, triggering the second load redistribution. After this redistribution, $Sw_2$'s load drops to 17.73. Then more load is added to $Sw_2$ until its load reaches the next new threshold 40 at $t_3 = 2008$h, triggering the third load redistribution. After this redistribution, $Sw_2$'s load drops to 23.27.

**Figure 6** illustrates the load changes of $Sw_2$ and the SAN reliability as the mission time proceeds. **Table 6** summarizes the load values of the five switches as well as the SAN reliability before and after each load redistribution under scheme 4, where the switches with the top three highest loads are selected for each load redistribution. During the first redistribution, $Sw_1$, $Sw_2$ and $Sw_5$ are selected; during the second redistribution, $Sw_2$, $Sw_4$ and $Sw_5$ are selected; during the third redistribution, $Sw_1$, $Sw_2$ and $Sw_3$ are selected (as highlighted in **Table 6**).

**Table 5.** Load and reliabilities of all the switches and the entire SAN under scheme 3.

| | Before redistribution | | | | | |
|---|---|---|---|---|---|---|
| | $t_1 = 1000$h | | $t_2 = 1571$h | | $t_3 = 2013$h | |
| | Load | Reliability | Load | Reliability | Load | Reliability |
| $Sw1$ | 15 | 0.9560405 | 11.33 | 0.9480197 | 22.91 | 0.8708643 |
| $Sw2$ | 50 | 0.7791900 | 45 | 0.7027080 | 40 | 0.6689084 |
| $Sw3$ | 5 | 0.8608370 | 9.333 | 0.6442941 | 13.44 | 0.4442876 |
| $Sw4$ | 1 | 0.9970074 | 17.44 | 0.9211215 | 35.36 | 0.8077798 |
| $Sw5$ | 8 | 0.9724155 | 24.44 | 0.8743083 | 17.92 | 0.8814389 |
| $Rsys$ | | 0.9692600 | 11.33 | 0.8907794 | | 0.8038852 |
| | After redistribution | | | | | |
| | Load | Reliability | Load | Reliability | Load | Reliability |
| $Sw1$ | 11.33 | 0.9666044 | 22.91 | 0.8977285 | 35.47 | 0.8072784 |
| $Sw2$ | 16.44 | 0.9213731 | 17.92 | 0.8691085 | 20.33 | 0.8154317 |
| $Sw3$ | 9.33 | 0.7559954 | 13.44 | 0.5309652 | 15.25 | 0.3983466 |
| $Sw4$ | 17.44 | 0.9490621 | 35.37 | 0.8465626 | 20.33 | 0.8845074 |
| $Sw5$ | 24.44 | 0.9180807 | 17.92 | 0.9062176 | 38.25 | 0.7638544 |
| $Rsys$ | | 0.9797992 | | 0.9319484 | | 0.8731286 |



**Figure 6.** The changes of SAN reliability and load of $Sw_2$ under scheme 4.

## 6.5 Comparisons and Discussions

As demonstrated in **Figures 3-6**, the SAN reliability may be improved significantly after each load reallocation process under the four proposed mitigation schemes. However, the effectiveness of the proposed schemes may be different and is compared in this section.

**Table 6.** Load and reliabilities of all the switches and the entire SAN under scheme 4.

| | Before redistribution | | | | | |
|---|---|---|---|---|---|---|
| | $t_1 = 1000h$ | | $t_2 = 1562h$ | | $t_3 = 2008h$ | |
| | Load | Reliability | Load | Reliability | Load | Reliability |
| $Sw_1$ | 15 | 0.9560405 | 12.67 | 0.9424070 | 25.96 | 0.8552829 |
| $Sw_2$ | 50 | 0.7791900 | 45 | 0.7041612 | 40 | 0.6695274 |
| $Sw_3$ | 5 | 0.8608370 | 14.67 | 0.5031636 | 27.96 | 0.1856950 |
| $Sw_4$ | 1 | 0.9970074 | 17.89 | 0.9196394 | 17.73 | 0.8987569 |
| $Sw_5$ | 8 | 0.9724155 | 16.88 | 0.9118567 | 17.73 | 0.8829090 |
| $R_{sys}$ | | 0.9692600 | | 0.8498434 | | 0.7217029 |
| | After redistribution | | | | | |
| | Load | Reliability | Load | Reliability | Load | Reliability |
| $Sw_1$ | 12.67 | 0.9627495 | 25.96 | 0.8855162 | 11.86 | 0.9310851 |
| $Sw_2$ | 16.89 | 0.9193299 | 17.73 | 0.8711162 | 23.27 | 0.7921504 |
| $Sw_3$ | 14.67 | 0.6443199 | 27.96 | 0.2699535 | 12.26 | 0.4780070 |
| $Sw_4$ | 17.89 | 0.9477988 | 17.73 | 0.9203308 | 40.99 | 0.7812609 |
| $Sw_5$ | 16.88 | 0.9426578 | 17.73 | 0.9076839 | 40.99 | 0.7497712 |
| $R_{sys}$ | | 0.9702458 | | 0.9006188 | | 0.8633420 |

## 6.5.1 Comparisons using Reliability Improvement Ratio

To evaluate and compare the effectiveness of different schemes, we calculate the average of SAN reliability improvement ratio (IR) based on Equation (11), where $n$ denotes the number of load redistributions triggered, $IR_i$ denotes the improvement ratio of redistribution $i$, $AR_i$ and $BR_i$ denote the SAN reliability after and before redistribution $i$, respectively.

$$IR_{average} = \frac{1}{n}\sum_{i=1}^{n} IR_i = \frac{1}{n}\sum_{i=1}^{n}\left[\frac{AR_i - BR_i}{BR_i}\right] \tag{11}$$

**Table 7** summaries the value of IR for each redistribution as well as the average IR value over the three redistributions (i.e., $n=3$).

**Table 7.** $IR$ comparison.

| | Scheme 1 | Scheme 2 | Scheme 3 | Scheme 4 |
|---|---|---|---|---|
| $IR_1$ | 0.0108 | 0.0010 | 0.0108 | 0.0010 |
| $IR_2$ | 0.0550 | 0.0772 | 0.0462 | 0.0598 |
| $IR_3$ | 0.1595 | 0.2960 | 0.0861 | 0.1962 |
| $IR_{average}$ | 0.0751 | 0.1247 | 0.0476 | 0.0857 |

Comparing the values of $IR_{average}$ under scheme 1 (0.0751) and scheme 3 (0.0476), it can be observed that the mitigation scheme using the static threshold outperforms the mitigation scheme using the dynamic threshold under the reliability-sensitive node selection rule. Comparing the values of $IR_{average}$ under scheme 2 (0.1247) and scheme 4 (0.0857), it can be observed that the mitigation scheme using the static threshold also outperforms the mitigation scheme using the dynamic threshold under the load-sensitive node selection rule.

Comparing the values of $IR_{average}$ under scheme 1 (0.0751) and scheme 2 (0.1247), it can be observed that the load-sensitive selection rule outperforms the reliability-sensitive selection rule under the mitigation schemes using the static threshold. Comparing the values of $IR_{average}$ under scheme 3 (0.0476) and scheme

4 (0.0857), it can be observed that the load-sensitive selection rule also outperforms the reliability-sensitive selection rule under the mitigation schemes using the dynamic threshold.

Based on the above comparisons, it can be concluded that in terms of $IR_{average}$ the mitigation scheme using the static threshold always outperforms the mitigation scheme using the dynamic threshold regardless of the selection rule adopted, and the load-sensitive selection rule always outperforms the reliability-sensitive selection rule.

### 6.5.2 Comparisons using SAN Reliability
To further evaluate and compare the effectiveness of different schemes, we present the SAN reliability values under different schemes at several common mission times.

To compare the performance of the two different node selection rules, we calculate the SAN reliability at $t = 2286h$ under static scheme 1 (0.7112488) and scheme 2 (0.7932698), and at $t = 2008h$ under dynamic scheme 3 (0.8055559) and scheme 4 (0.8633420). Under both static and dynamic threshold schemes, the load-sensitive selection rule outperforms the reliability-sensitive selection rule.

To compare the performance of the static and dynamic threshold mitigation schemes, we calculate the SAN reliability at $t = 2013h$ under scheme 1 (0.8104713) and scheme 3 (0.8731286), and at $t = 2008h$ under scheme 2 (0.7396682) and scheme 4 (0.8633420). Under both reliability-sensitive and load-sensitive node selection rules, the mitigation scheme using the dynamic threshold outperforms the mitigation scheme using the static threshold in terms of the resulting SAN reliability.

## 7. Effects of Step Value in Dynamic Threshold Mitigation Schemes
To study the effect of the step value (i.e., the value of $s$) on the performance of the mitigation schemes using dynamic thresholds, we perform the numerical studies using a different step value $s = 10$ in this section and compare the results with those in Section 6. where, $s = 5$ is used.

### 7.1 Dynamic Scheme 3 with $s = 10$
Similar to Section 6, we increase the load of $Sw_2$ from 0 to 50 as mission time $t$ proceeds based on Equation (10) while using initial load value in **Table 2** for all other switches. At $t_1 = 1000h$, the load of $Sw_2$ reaches the initial threshold of 50, triggering the load redistribution. After the redistribution, $Sw_2$'s load drops to 16.44. Following Equation (10), more load is added to $Sw_2$ until its load reaches the new threshold $(50-s) = 40$ at $t_2 = 1471h$, triggering the second load redistribution. After this redistribution, $Sw_2$'s load drops to 16.81. Then more load is added to $Sw_2$ until its load reaches the next new threshold $(40-s) = 30$ at $t_3 = 1735h$, triggering the third load redistribution. After this redistribution, $Sw_2$'s load drops to 17.64.

**Figure 7** illustrates the load changes of $Sw_2$ and the SAN reliability as the mission time proceeds. **Table 8** summarizes the load values of the five switches as well as the SAN reliability before and after each load redistribution under Scheme 3, where the switches with the top three lowest reliabilities are selected for each load redistribution. During the first redistribution, $Sw_1$, $Sw_2$ and $Sw_3$ are selected; during the second redistribution, $Sw_2$, $Sw_3$ and $Sw_5$ are selected; during the third redistribution, $Sw_2$, $Sw_3$ and $Sw_4$ are selected (as highlighted in **Table 8**).
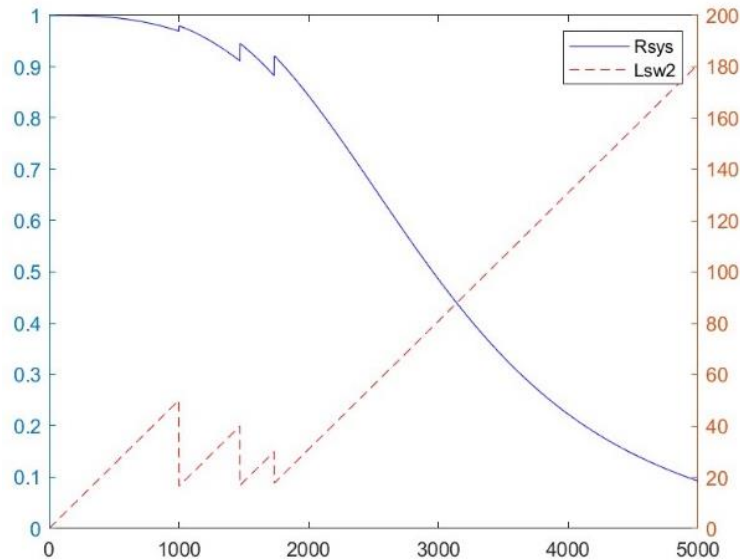
**Figure 7.** The changes of SAN reliability and load of $Sw_2$ under scheme 3 ($s = 10$).

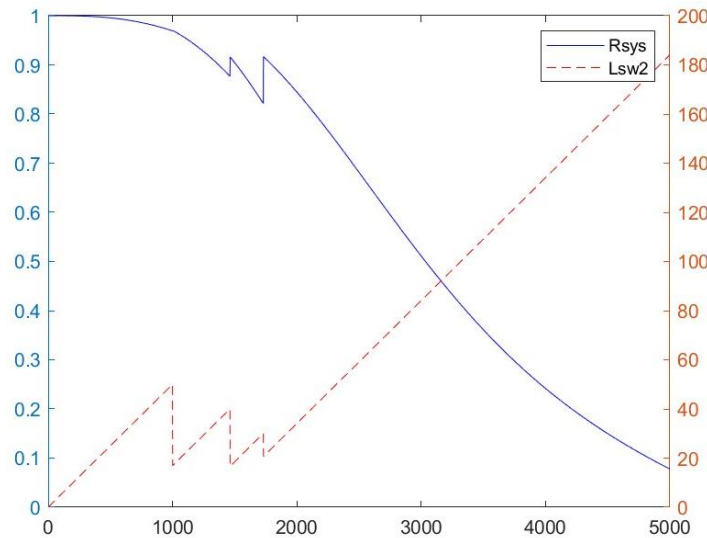**Table 8.** Load and reliabilities of all the switches and the entire SAN under scheme 3 ($s$=10).

| | Before redistribution | | | | | |
|---|---|---|---|---|---|---|
| | $t_1$=1000h | | $t_2$=1471h | | $t_3$=1735h | |
| | Load | Reliability | Load | Reliability | Load | Reliability |
| $Sw_1$ | 15 | 0.9560405 | 11.33 | 0.9512484 | 23.94 | 0.8829032 |
| $Sw_2$ | 50 | 0.7791900 | 40 | 0.7455809 | 30 | 0.7712427 |
| $Sw_3$ | 5 | 0.8608370 | 9.333 | 0.6625893 | 12.61 | 0.5190073 |
| $Sw_4$ | 1 | 0.9970074 | 17.44 | 0.9259547 | 34.25 | 0.8367826 |
| $Sw_5$ | 8 | 0.9724155 | 24.44 | 0.8818206 | 16.81 | 0.9030123 |
| $R_{sys}$ | | 0.9692600 | | 0.9112403 | | 0.8825592 |
| | After redistribution | | | | | |
| | Load | Reliability | Load | Reliability | Load | Reliability |
| $Sw_1$ | 11.33 | 0.9666044 | 23.94 | 0.8998037 | 34.65 | 0.8350629 |
| $Sw_2$ | 16.44 | 0.9213731 | 16.81 | 0.8841000 | 17.64 | 0.8585490 |
| $Sw_3$ | 9.33 | 0.7559954 | 12.61 | 0.5735061 | 13.23 | 0.5024534 |
| $Sw_4$ | 17.44 | 0.9490621 | 34.25 | 0.8597948 | 17.64 | 0.9123177 |
| $Sw_5$ | 24.44 | 0.9180807 | 16.81 | 0.9171476 | 34.45 | 0.8113298 |
| $R_{sys}$ | | 0.9797992 | | 0.9456726 | | 0.9215826 |

## 7.2 Dynamic Scheme 4 with $s = 10$

Similarly, under scheme 4, we increase the load of $Sw_2$ from 0 to 50 as mission time $t$ proceeds based on Equation (10) while using initial load value in **Table 2** for all other switches. At $t_1 = 1000$h, the load of $Sw_2$ reaches the initial threshold of 50, triggering the load redistribution. After the redistribution, $Sw_2$'s load drops to 16.89. Following Equation (10), more load is added to $Sw_2$ until its load reaches the new threshold 40 at $t_2 = 1462$h, triggering the second load redistribution. After this redistribution, $Sw_2$'s load drops to 16.61. Then more load is added to $Sw_2$ until its load reaches the next new threshold 30 at $t_3 = 1730$h, triggering the third load redistribution. After this redistribution, $Sw_2$'s load drops to 20.60.

**Figure 8** illustrates the load changes of $Sw_2$ and the SAN reliability as the mission time proceeds. **Table 9** summarizes the load values of the five switches as well as the SAN reliability before and after each load

redistribution under scheme 4, where the switches with the top three highest loads are selected for each load redistribution. During the first redistribution, $Sw_1$, $Sw_2$ and $Sw_5$ are selected; during the second redistribution, $Sw_2$, $Sw_4$ and $Sw_5$ are selected; during the third redistribution, $Sw_1$, $Sw_2$ and $Sw_3$ are selected (as highlighted in **Table 9**).



**Figure 8.** The changes of SAN reliability and load of $Sw_2$ under scheme 4 ($s = 10$).

**Table 9.** Load and reliabilities of all the switches and the entire SAN under scheme 4 ($s = 10$).

| | Before redistribution | | | | | |
|---|---|---|---|---|---|---|
| | $t_1 = 1000$h | | $t_2 = 1462$h | | $t_3 = 1730$h | |
| | Load | Reliability | Load | Reliability | Load | Reliability |
| $Sw_1$ | 15 | 0.9560405 | 12.67 | 0.9459950 | 25.13 | 0.8777904 |
| $Sw_2$ | 50 | 0.7791900 | 40 | 0.7469526 | 30 | 0.7717712 |
| $Sw_3$ | 5 | 0.8608370 | 14.67 | 0.5257970 | 27.13 | 0.2448244 |
| $Sw_4$ | 1 | 0.9970074 | 17.89 | 0.9245880 | 16.62 | 0.9174164 |
| $Sw_5$ | 8 | 0.9724155 | 16.89 | 0.9172627 | 16.62 | 0.9043313 |
| $R_{sys}$ | | 0.9692600 | | 0.8770859 | | 0.8218472 |
| | After redistribution | | | | | |
| | Load | Reliability | Load | Reliability | Load | Reliability |
| $Sw_1$ | 12.67 | 0.9627495 | 25.13 | 0.8957059 | 10.03 | 0.9493246 |
| $Sw_2$ | 16.89 | 0.9193299 | 16.61 | 0.8860127 | 20.60 | 0.8372136 |
| $Sw_3$ | 14.67 | 0.6443199 | 27.13 | 0.3044977 | 10.43 | 0.5822864 |
| $Sw_4$ | 17.89 | 0.9477988 | 16.62 | 0.9297556 | 37.22 | 0.8244334 |
| $Sw_5$ | 16.89 | 0.9426578 | 16.62 | 0.9185376 | 37.22 | 0.7983283 |
| $R_{sys}$ | | 0.9702458 | | 0.9167890 | | 0.9173340 |

## 7.3 Comparisons and Discussions
### 7.3.1 Comparisons using Reliability Improvement Ratio
**Table 10** summarizes the values of $IR_{average}$ under different step values using scheme 3 and scheme 4. It can be observed that as the step value increases, the performance of dynamic mitigation schemes becomes worse or less effective in terms of the reliability improvement ratio. Comparing the values of $IR_{average}$ under scheme 3 and scheme 4 with the same value of $s$, the dynamic mitigation schemes using the load-

sensitive selection rule outperform the dynamic mitigation schemes using the reliability-sensitive selection rule.

**Table 10.** IR comparison of schemes 3 and 4 under different step values.

| | Scheme 3 | | Scheme 4 | |
|---|---|---|---|---|
| | $s = 5$ | $s = 10$ | $s = 5$ | $s = 10$ |
| $IR_1$ | 0.0108 | 0.0109 | 0.0010 | 0.0011 |
| $IR_2$ | 0.0462 | 0.0377 | 0.0598 | 0.0453 |
| $IR_3$ | 0.0861 | 0.0442 | 0.1962 | 0.1162 |
| $IR_{average}$ | 0.0476 | 0.0310 | 0.0857 | 0.0542 |

### 7.3.2 Comparisons using SAN Reliability

To further investigate the effects of the step value (i.e., the value of $s$), we calculate the SAN reliability at $t = 1735$ for $s = 5$ (0.8897228) and $s = 10$ (0.9215826) under scheme 3 and the SAN reliability at $t = 1730$ for $s = 5$ (0.8388160) and $s = 10$ (0.9173340) under scheme 4. It is clear that as the step value increases, the dynamic schemes tend to perform more effectively in terms of the resulting SAN reliability.

## 8. Conclusion and Future Work

This paper suggests four types of load redistribution schemes triggered by the overload of certain switch to mitigate the risk of cascading failures in SAN systems. Static and dynamic thresholds are considered for triggering the load redistribution. Load-sensitive and reliability-sensitive rules are considered for selecting nodes to participate in each load redistribution. A detailed case study of a mesh SAN has been conducted to evaluate and compare the performance of the proposed mitigation schemes using criteria of SAN reliability improvement ratio and the resulting SAN reliability.

It has been revealed from the case study that Equation (1) in terms of the average reliability improvement ratio, the mitigation scheme using the static threshold always outperforms the mitigation scheme using the dynamic threshold regardless of the node selection rule adopted; Equation (2) in terms of the resulting SAN reliability, the mitigation scheme using the dynamic threshold outperforms the mitigation scheme using the static threshold regardless of the node selection rule adopted; and Equation (3) in terms of both the average reliability improvement ratio and the resulting SAN reliability, the load-sensitive selection rule always outperforms the reliability-sensitive selection rule. For the mitigation schemes using dynamic thresholds, the effects of the step value have also been investigated. It is revealed that as the step value increases, the dynamic mitigation schemes become less effective in terms of the average reliability improvement ratio but more effective in terms of the resulting SAN reliability.

In the future, based on the SAN reliability and other performance metrics (like throughput and response time), we plan to explore comprehensive resilience metrics for SANs and investigate effective mitigation schemes to build the resilience of SANs against cascading failures (Xing, 2020, 2024).

# Reference

Al-Aqqad, W., Hayajneh, H., & Zhang, X. (2023). A simulation study of the resiliency of mobile energy storage networks. *Processes*, *11*(3), 762. https://doi.org/10.3390/pr11030762.

Bialek, J., Ciapessoni, E., Cirio, D., Citilla-Sanchez, E., Dent, C., Dobson, I., Henneaux, P., Hines, P., Jardim, J., Miller, S., Panteli, M., Papic, M., Pitto, A., Quiros-Tortos, J., & Wu, D. (2016). Benchmarking and validation of cascading failure analysis tools. *IEEE Transactions on Power Systems*, *31*(6), 4887-4900. https://doi.org/10.1109/tpwrs.2016.2518660.

Dang, Y., Yang, L., He, P., & Guo, G. (2023). Effects of collapse probability on cascading failure dynamics for duplex weighted networks. *Physica A: Statistical Mechanics and its Applications*, *626*, 129069. https://doi.org/10.1016/j.physa.2023.129069.

DELL EMC Corporation. (2019). Dell EMC VMAX3 Family Product Guide. Available: https://www.delltechnologies.com/asset/en-us/products/storage/technical-support/docu59438.pdf. Accessed in May 2024.

Dey, P., Mehra, R., Kazi, F., Wagh, S., & Singh, N.M. (2016). Impact of topology on the propagation of cascading failure in power grid. *IEEE Transactions on Smart Grid*, *7*(4), 1970-1978. https://doi.org/10.1109/tsg.2016.2558465.

Ed-daoui, I., El Hami, A., Itmi, M., Hmina, N., & Mazri, T. (2019). Resilience assessment as a foundation for systems-of-systems safety evaluation*:* Application to an economic infrastructure. *Safety Science*, *115*, 446-456. https://doi.org/10.1016/j.ssci.2019.02.030.

EMC Corporation (2009). *EMC connectrix B series ED-DCX-4S-B version 6.2 hardware reference manual*. Available: https://www.manualslib.com/manual/1802339/emc-connectrix-b-series.html?page=3#manual. Accessed in May 2024.

Garber, L. (2012). Converged infrastructure: Addressing the efficiency challenge. *Computer*, *45*(8), 17-20. https://doi.org/10.1109/mc.2012.261.

Ghorbani-Renani, N., González, A.D., Barker, K., & Morshedlou, N. (2020). Protection-interdiction-restoration: Tri-level optimization for enhancing interdependent network resilience. *Reliability Engineering & System Safety*, *199*, 106907. https://doi.org/10.1016/j.ress.2020.106907.

Harpel, B.M., Dugan, J.B., Walker, I.D., & Cavallaro, J.R. (1997). Analysis of robots for hazardous environments. In *Proceedings of Annual Reliability and Maintainability Symposium* (pp. 111-116). IEEE. Philadelphia, PA, USA. https://doi.org/10.1109/rams.1997.571676.

Huang, Q., Shao, L., & Li, N. (2016). Dynamic detection of transmission line outages using hidden Markov models. *IEEE Transactions on Power Systems*, *31*(3), 2026-2033. https://doi.org/10.1109/tpwrs.2015.2456852.

Hutanu, A., Allen, G., & Kosar, T. (2010). High-performance remote data access for remote visualization. In *2010 11th IEEE/ACM International Conference on Grid Computing* (pp. 121-128). IEEE. Brussels, Belgium. https://doi.org/10.1109/grid.2010.5697967.

Jacob, V., & Prakash, M. (2022). A review of big data analytics on post-COVID health issues. In *Proceedings of IEEE International Conference on Recent Advances and Innovations in Engineering* (pp. 138-143. IEEE. Mangalore, India. https://doi.org/10.1109/icraie56454.2022.10054317.

Kay, R., & Kinnersley, N. (2002) On the use of the accelerated failure time model as an alternative to the proportional hazards model in the treatment of time to event data: a case study in influenza. *Drug Information Journal, 36*(3), 571-579. https://doi.org/10.1177/009286150203600312.

Levitin, G., & Amari, S.V. (2009). Optimal load distribution in series-parallel systems. *Reliability Engineering & System Safety*, *94*(2), 254-260. https://doi.org/10.1016/j.ress.2008.03.001.

Li, J., Wang, Y., & Zhong, J. (2022a). An exceeding recovery model for enhancing network resilience against cascading failures. *IEEE Access*, *10*, 71035-71043. https://doi.org/10.1109/access.2022.3188659.

Li, J., Wang, Y., Zhong, J., Sun, Y., Guo, Z., Chen, Z., & Fu, C. (2022b). Network resilience assessment and reinforcement strategy against cascading failure. *Chaos, Solitons & Fractals*, *160*, 112271. https://doi.org/10.1016/j.chaos.2022.112271.

Liu, C., Li, D., Zio, E., & Kang, R. (2014). A modeling framework for system restoration from cascading failures. *PloS one*, *9*(12), e112363. https://doi.org/10.1371/journal.pone.0112363.

Liu, D., Zhang, X., & Tse, C.K. (2022). Effects of high level of penetration of renewable energy sources on cascading failure of modern power systems. *IEEE Journal on Emerging and Selected Topics in Circuits and Systems*, *12*(1), 98-106. https://doi.org/10.1109/jetcas.2022.3147487.

Lv, G, & Xing, L. (2021). Influence of load on reliability of storage area networks. *International Journal of Mathematical, Engineering and Management Sciences*, *6*(6), 1533-1552. https://doi.org/10.33889/ijmems.2021.6.6.091.

Lv, G., Xing, L., Wang, H., & Liu, H. (2023). Load redistribution-based reliability enhancement for storage area networks. *International Journal of Mathematical, Engineering and Management Sciences*, *8*(1), 1-14. https://doi.org/10.33889/ijmems.2023.8.1.001.

Mishra, S., Anderson, K., Miller, B., Boyer, K., & Warren, A. (2020). Microgrid resilience: A holistic approach for assessing threats, identifying vulnerabilities, and designing corresponding mitigation strategies. *Applied Energy*, *264*, 114726. https://doi.org/10.1016/j.apenergy.2020.114726.

Nguyen, T.N., Liu, B.H., Nguyen, N.P., Dumba, B., & Chou, J.T (2021). Smart grid vulnerability and defense analysis under cascading failure attacks. *IEEE Transactions on Power Delivery*, *36*(4), 2264-2273. https://doi.org/10.1109/tpwrd.2021.3061358.

Rahnamay-Naeini, M., & Hayat, M.M. (2016). Cascading failures in interdependent infrastructures: An interdependent Markov-chain approach. *IEEE Transactions on Smart Grid*, *7*(4), 1997-2006. https://doi.org/10.1109/tsg.2016.2539823.

Sharma, M., Luthra, S., Joshi, S., & Kumar, A. (2022). Developing a framework for enhancing survivability of sustainable supply chains during and post-COVID-19 pandemic. *International Journal of Logistics Research and Applications*, 25(4-5), 433-453. https://doi.org/10.1080/13675567.2020.1810213.

Shi, L., Shi, Z., Yao, L., Ni, Y., & Bazarga, M. (2010). A review of mechanism of large cascading failure blackouts of modern power system. *Power System Technology*, *34*(3), 48-54.

Simache, C., & Kaaniche, M. (2005). Availability assessment of sunOS/solaris unix systems based on syslogd and wtmpx log files: A case study. In *Proceedings of IEEE Pacific Rim International Symposium on Dependable Computing* (pp. 8). IEEE. Hunan, China. https://doi.org/10.1109/prdc.2005.20.

Wang, J., Rong, L., Zhang, L., & Zhang, Z. (2008). Attack vulnerability of scale-free networks due to cascading failures. *Physica A: Statistical Mechanics and its Applications*, *387*(26), 6671-6678. https://doi.org/10.1016/j.physa.2008.08.037.

Xing, L. (2020). Reliability in internet of things: Current status and future perspectives. *IEEE Internet of Things Journal*, *7*(8), 6704-6721. https://doi.org/10.1109/jiot.2020.2993216.

Xing, L. (2021). Cascading failures in internet of things: Review and perspectives on reliability and resilience. *IEEE Internet of Things Journal*, *8*(1), 44-64. https://doi.org/10.1109/jiot.2020.3018687.

Xing, L. (2024). *Reliability and resilience in the internet of things.* Elsevier. ISBN: 9780443156113.

Xing, L., & Amari, S.V. (2015). *Binary decision diagrams and extensions for system reliability analysis*. Wiley-Scrivener, MA, USA.

Xing, L., & Dugan, J.B. (2002). Analysis of generalized phased mission system reliability, performance and sensitivity. *IEEE Transactions on Reliability*, *51*(2), 199-211. https://doi.org/10.1109/tr.2002.1011526.

Xing, L., Morrissette, B.A., & Dugan, J.B. (2014). Combinatorial reliability analysis of imperfect coverage systems subject to functional dependence. *IEEE Transaction on Reliability*, *63*(1), 367-382. https://doi.org/10.1109/tr.2014.2299431.

Xing, L., Tannous, M., Vokkarane, V.M., Wang, H., & Guo J. (2017). Reliability modeling of mesh storage area networks for Internet of things. *IEEE Internet of Things Journal*, *4*(6), 2047-2057. https://doi.org/0.1109/jiot.2017.2749375.

Zhou, J., Coit, D.W., Felder, F.A., & Wang, D. (2021). Resiliency-based restoration optimization for dependent network systems against cascading failures. *Reliability Engineering & System Safety*, *207*, 107383. https://doi.org/10.1016/j.ress.2020.107383.

**Publisher's Note**- Ram Arti Publishers remains neutral regarding jurisdictional claims in published maps and institutional affiliations.